

Article

Experimental Study on the Fracturing Behaviors and Mechanical Properties of Cracks under Coupled Hydro-Mechanical Effects in Rock-like Specimens

Yimeng Zhou ¹, Cheng Zhao ^{1,2,*}, Chunfeng Zhao ¹, Chuangchuang Ma ¹ and Junfei Xie ¹

¹ Department of Geotechnical Engineering, College of Civil Engineering, Tongji University, Shanghai 200092, China; zhouyimeng52@163.com (Y.Z.); tjzhchf@tongji.edu.cn (C.Z.); 13162200872@163.com (C.M.); 18321863927@163.com (J.X.)

² College of Engineering, Tibet University, Lhasa 850011, China

* Correspondence: zhaocheng@tongji.edu.cn; Tel.: +86-138-1884-0876

Received: 12 September 2018; Accepted: 27 September 2018; Published: 29 September 2018



Abstract: The artificial fracturing technique under coupled hydro-mechanical effects is widely used in many rock engineering. Therefore, the study on the fracturing behaviors and mechanical properties of hydro-mechanical coupled cracks is very crucial. In this study, a series of fracturing tests were conducted on the cylinder gypsum specimens with single pre-existing cracks using triaxial compression loading system. Water pressure was applied inside the pre-existing cracks and led to the specimen failure with external compression loading. A new type of cracks, namely horizontal coupled cracks (HCC), were found in some specimens. Macroscopic observations reveal that HCC, which were mainly caused by the hydraulic pressure, were different from any tensile wing cracks, shear secondary cracks, or shear anti-wing cracks. Subsequently, a microscopic study was performed using scanning electron microscope (SEM), the outcomes suggest that: (1) Shear fracturing zones (SFZ) and tensile fracturing zones (TFZ) under coupled hydro-mechanical effects displayed distinct characteristics on orientations, length, and independence of gypsum grains; and (2) the HCC were tensile cracks when they just initiated from outer tips of pre-existing cracks. While tensile stress made major contribution to the specimen failure during the whole fracturing processes, the HCC became tensile and shear mixed cracks when the specimen was about to fail.

Keywords: Coupled hydro-mechanical effect; triaxial compression loading test; microscopic observation; tensile and shear properties

1. Introduction

Crack fracturing under coupled hydro-mechanical effects is a widely used method for creating cracks in deep rock formation and enhancing hydraulic conductivity of geological reservoirs. Despite this important technique, it is routinely adopted in oil and gas extraction and enhanced geothermal systems, the fracturing behaviors, and mechanical properties of hydro-mechanical coupled cracks are not comprehensively understood [1]. In order to better investigate the basic hydro-mechanical fracturing mechanism, many experimental tests have been carried out.

For convenience, in the introduction part, the term “hydraulic cracks” represents all types of the cracks under coupled hydro-mechanical effects. Among all the rock materials, sandstone is the most widely used material in hydro-mechanical fracturing [2–9]. For example, Warpinski [10] researched the effect of geologic discontinuities on the propagation of hydraulic cracks. A fracture interaction criterion was proposed to forecast the occurrence of shear slippage on the natural fracture plane which caused by the induced fracture. Blair et al. [11] presented a series of studies on the hydraulic fracture propagation into and through an interface. Damani et al. [12] investigated complex hydraulic

fracturing processes of Lyons sandstone on a micro level. Wanniarachchi et al. [13] studied the influence of confining pressure and injection pressure on the permeability of hydraulically fractured specimens. Besides the sandstone, many other rock materials were also adopted to the hydraulic experimental tests, such as limestone [14,15], coal [16,17], shale [18–22], and granite [23–28]. Blanton et al. [29] systematically studied the relationships between hydraulic propagating fractures and natural fractures using Devonian shale. The results showed that the hydraulic cracks would cross the pre-existing cracks only under high differential stress conditions and high approach angle. Li et al. [20] carried out hydraulic tests in shale cores with diverse stress statuses and environment conditions. Lin et al. [21] experimentally investigated the effects of the anisotropy of shale during hydraulic fracturing processes. Gonçalves da Silva and Einstein [1] investigated the effect of vertical load and fracture geometries on the physical propagation processes and coalescence patterns of hydraulically-created cracks in granite. Due to the quick and easy preparation of the specimens, artificial materials have also been widely used to study the development of hydraulic fractures [30–34]. Zhou et al. [35,36] conducted triaxial compression loading tests to study the propagation behaviors and fracture geometry in man-made specimens. Three interaction types were proposed, and the interference factors of hydraulic fracture orientations were analyzed. Amalokwu et al. [37] studied the effect of saturated cracks in synthetic rock specimens, the results showed that the presence of air-water cracks significantly influence the shear waves. Liu et al. [38] estimated the hydraulic properties and size effect of single fractures filled with different graded and gap-graded fillings.

However, hydro-mechanical fracturing is an exceedingly complicated process, which is affected by many controllable or uncontrollable factors such as the mechanical properties of rock (strength, stiffness, saturation, porosity, and size of grains), the statuses of fracturing fluid (type, viscosity, temperature, and injection rate), external stress states, and geometry of pre-existing cracks. Even at present, there is still no unified conclusions on some issues, for example, the influence of hydraulic pressure on the cracking trajectories and the tensile and shear properties of hydro-mechanical coupled cracks.

In this paper, the fracturing behaviors and mechanical properties of coupled cracks in cylinder rock-like specimens are investigated and analyzed. A series of experimental tests are conducted under triaxial compression loading system and scanning electron microscope (SEM). This paper first briefly introduces the specimen preparation and the test setup. Then, the macroscopic results are discussed on the observation of the fracturing trajectories. Subsequently, the tensile and shear properties of coupled cracks are studied on a micro scale. Finally, summaries and conclusions are provided towards the end of the paper.

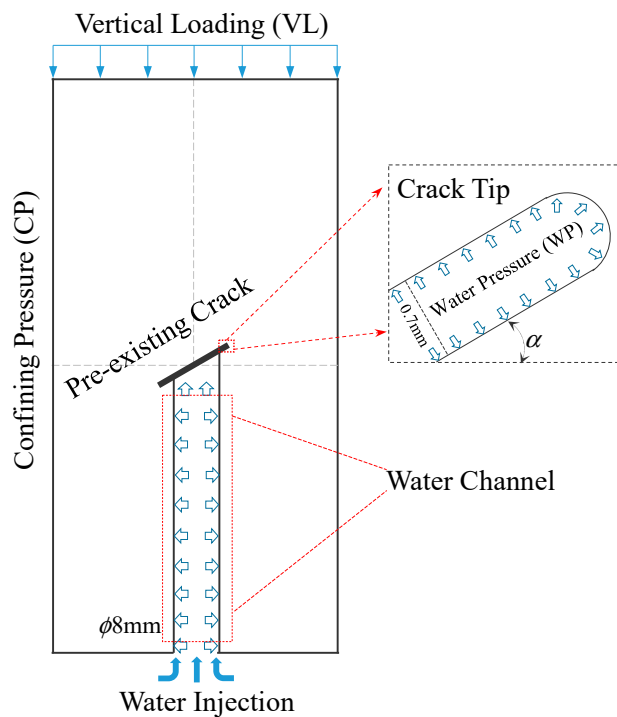
2. Materials and Methods

2.1. Specimen Preparation

The cylinder gypsum specimens (Table 1) used in the fracturing tests were $\phi 50 \text{ mm} \times 100 \text{ mm}$, and the crack length and aperture were 14 mm and 0.7 mm, respectively. The specimens are comprised a mixture of gypsum, water, and retarder in the ratio by weight of 1:0.35:0.005. To generate single pre-existing crack, a piece of mica sheet ($60 \times 14 \times 0.7 \text{ mm}^3$) is placed into slots in the mold template and remained in the specimen during curing. To create different crack inclination angles, the orientations of the mica sheet are predetermined and can be adjusted with the slots. As shown in Figure 1, in order to fill the pre-existing cracks with water pressure, a hydraulic channel with a diameter of 8mm was drilled in advance. This hydraulic channel was in the middle of the specimen along the vertical direction from the bottom to the pre-cracks. The inclination angle of pre-existing crack (α) varied from 15° to 75° in 15° increments. In the present study, '30° specimen' denotes the specimen for which α is 30° .

Table 1. Specimen's parameters.

ρ (g/cm ³)	E (MPa)	ν	σ_c (MPa)	σ_t (MPa)	c (MPa)	φ (°)
2.38	15,000	0.23	39.80	1.40	10.44	30

**Figure 1.** Loading conditions used in the hydraulic fracturing tests.

2.2. Test Setup and Procedures

The macroscopic experiments in this study were conducted using a GCTS RTX-3000 triaxial rock testing system (Figure 2), which is housed in Tongji University, China. This testing system consists of a uniaxial compression loading system, a loading rack with slippery tracks, a triaxial pressure chamber, two confining pressure superchargers, a pore pressure supercharger, a microprocessor, and an analysis system. The uniaxial compression and confining pressure are applied using a piston mounted inside the confining vessel and the confining hydraulic oil, respectively. The fracturing fluid can be injected inside the specimens simultaneously inside the pressure chamber.

Figure 3 shows the specimen with the experimental devices installed. The measurement accuracy of the vertical displacement LVDT sensors and the radial displacement sensor are 0.001 mm. The procedure to perform the hydro-mechanical fracturing experiment is divided into five steps. First, adjust the pressure cushion to reach the boundary of the specimen, and ensure the reading of displacement sensors are 0. Second, apply the confining pressure to the target level at a rate of 0.1 MPa/s. Third, inject the fracturing water at a constant rate of 0.2 mL/s into the specimen through the water channel, the constant injection will last 5 min after the water pressure reaches the target level. Fourth, apply the vertical loading to the specimen using displacement control at a rate of 0.1 mm/min until the specimen failure. Finally, export the test data, which are recorded at a rate of 10 Hz, and unload the water pressure, the confining pressure, and the axial pressure alternately. In this study, the confining pressure was 6 MPa, and two hydraulic pressure values (0 MPa and 5 MPa) were applied to the specimens with the same inclination angles.



Figure 2. GCTS RTX-3000 triaxial rock testing system.

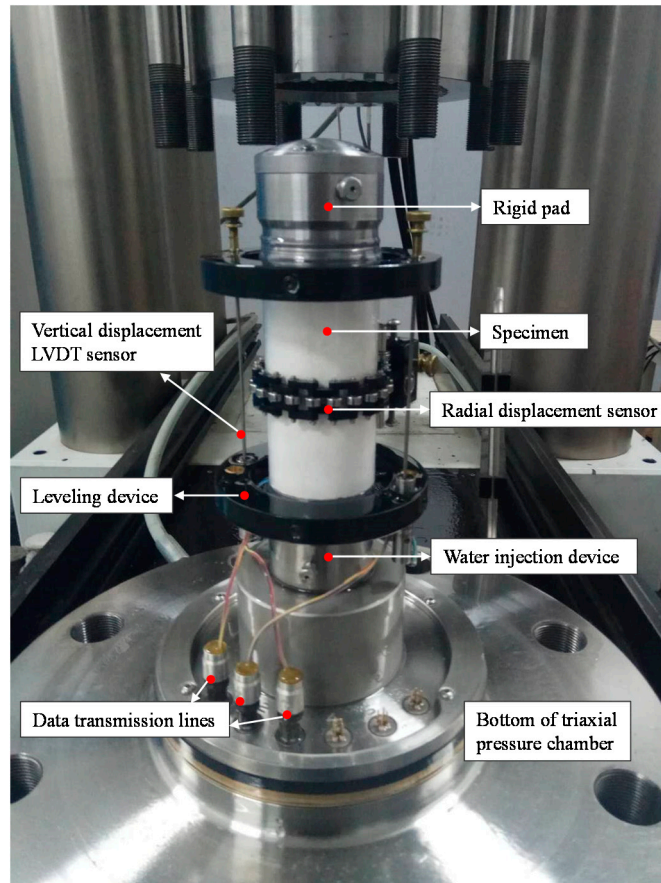


Figure 3. Photograph of experimental devices installed.

In order to investigate the mechanical properties of hydro-mechanical coupled cracks on a micro-scale, a scanning electron microscope (SEM) test was then carried out. The SEM system, Nova NanoSEM 450, in Tongji University was used for this study (Figure 4). The failure specimens were trimmed down to appropriate sizes (10 mm wide \times 5 mm thick \times 8 mm high), and a gold coating was applied to the fracture surfaces of the specimens before being placed in the SEM. In order to improve the clarity and accuracy of the scanning images, the SEM system was operated under the accelerating voltage of 10 KV. Thus, the measuring error caused by electronic reflection was reduced to 1.2 nm.

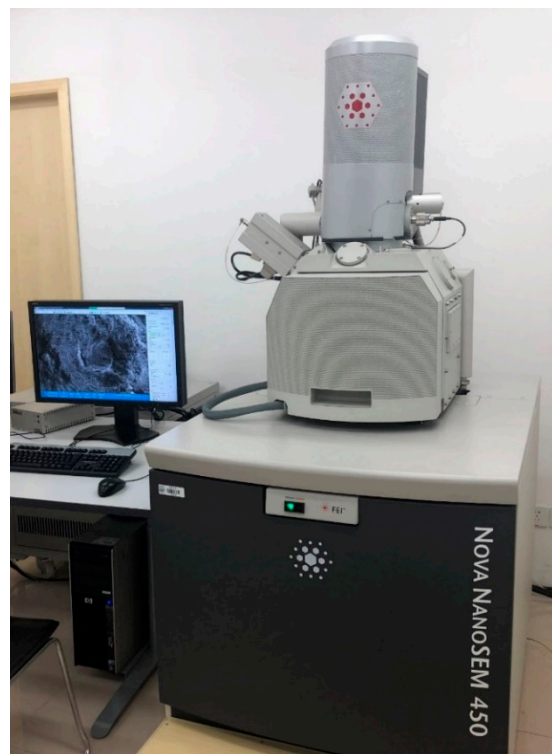


Figure 4. SEM system-Nova NanoSEM 450.

3. Macroscopic Study

3.1. Trajectories of Dry Cracks

Throughout this section, the terms “dry cracks” and “coupled cracks” are adopted. Dry cracks represent the cracks occurred in the specimens with no water pressure applied, including pre-existing cracks and new cracks developed in respond to the external loading. In contrast, coupled cracks represent the cracks which water pressure was applied on their surfaces, and the initiation and propagation of new cracks were caused by the coupling hydro-mechanical effects. Table 2 presents the cracks trajectories of both dry cracks (left) and coupled cracks (right).

As shown in the left column of Table 2, the failure statuses and crack trajectories of dry cracks are quite similar to the outcomes of uniaxial compression loading tests [39] and numerical simulation results. There was no secondary cracks or anti-wing cracks occurred, but only two primary cracks developed from the crack tips throughout the whole loading processes no matter how large the inclination angle was. It should be noted that these primary cracks were not simply equivalent to wing cracks even if they were similar on crack trajectories. Wong and Einstein [40] proposed that wing crack is an item to describe the shape of crack pattern and it should be only used for tensile cracks. When the primary cracks initiated, tensile properties of them were predominant. However, with the cracking propagation, shear properties of these cracks became more and more obvious. Moreover, in some specimens with large inclination angles, like 60° specimen and 75° specimen, shear cracks would initiate from the outer

tips of pre-existing cracks and led to the specimen failure. Actually, the primary dry cracks in this paper consisted of tensile cracks, shear cracks, and mixed cracks. Based on our previous experimental and numerical study [39,41], the types of dry cracks can be separated by macroscopic observation and analysis on the tensile/shear strain field. Considering this is not the focus of this paper, the mechanical properties and crack nature of dry cracks are directly marked in Table 2 without more analysis ('T' for tensile cracks and 'S' for shear cracks). While both the tensile cracks and shear cracks can be further divided into many subtypes, this paper only use items tensile and shear in the figures.

Table 2. Fracturing trajectories of dry cracks and coupled cracks.

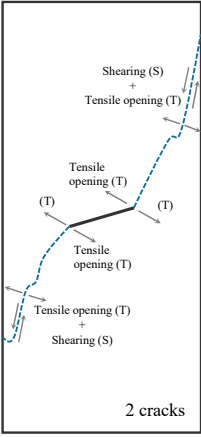
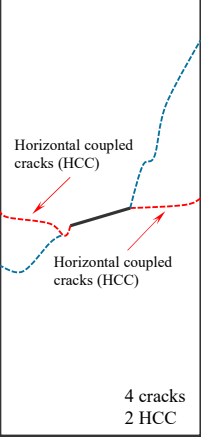
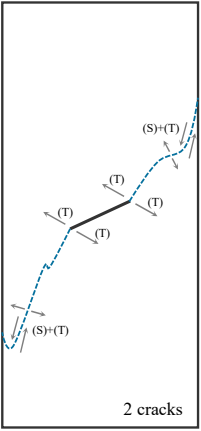
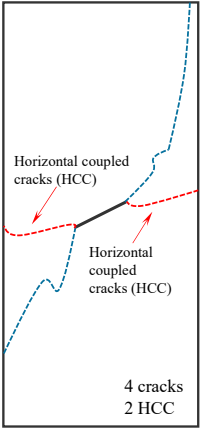
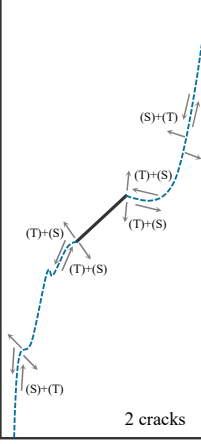
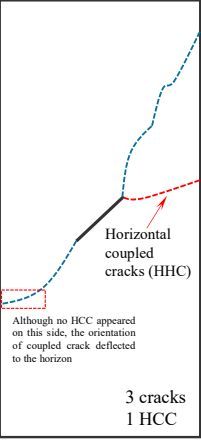
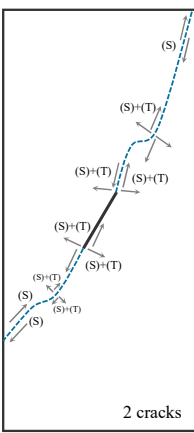
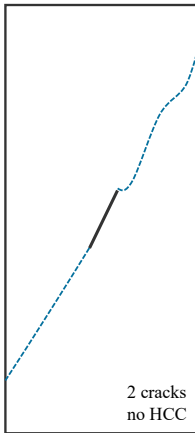
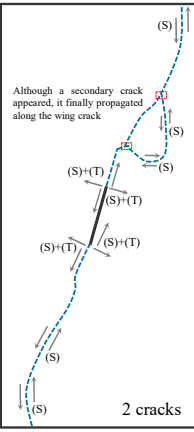
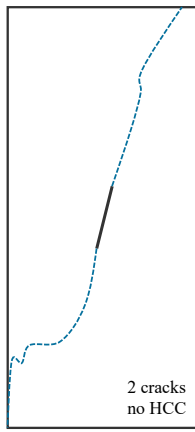
α	Water Pressure (WP) = 0 MPa	Water Pressure (WP) = 5 MPa
15°	 	 
30°	 	 
45°	 	 

Table 2. Cont.

α	Water Pressure (WP) = 0 MPa	Water Pressure (WP) = 5 MPa
60°	  <p>2 cracks</p>	  <p>2 cracks no HCC</p>
75°	  <p>2 cracks</p>	  <p>2 cracks no HCC</p>

3.2. Trajectories of Dry Cracks

Due to the hydro-mechanical coupling effect, the fracturing behaviors of coupled cracks are extremely complicated and different from those of dry cracks. Therefore, our previous findings cannot be directly applied to predict the propagation trajectories and crack types. Referring again to Table 2, when inclination angles were 15°, 30°, and 45°, new types of cracks were observed. They were horizontal coupled cracks (HCC), which are highlighted in red font in the figures. These HCC all initiated from the tips of pre-existing cracks and propagated towards the horizontal direction regardless of the effect of vertical loading and confining pressure. It should be noted that HCC were different from traditional secondary cracks or anti-wing cracks that appeared in uniaxial/biaxial compression loading tests. Firstly, HCC developed along the shortest path to the edges and the crack trajectories can be predicted. However, the trajectories of secondary cracks or anti-wing cracks were not well defined until final failure. Secondly, HCC only occurred in the specimens with low inclination angles, and the number of them decreased as inclination angles increased. In contrast, secondary or anti-wing cracks tend to initiate and propagate in specimens with large inclination angles, the number of subcoplanar cracks or oblique cracks are positively correlated with the inclination angles. Since the HCC were the special cracks mainly produced by coupling hydro-mechanical effects, their mechanical properties should be well studied.

In general, the mechanical properties of cracks can be reflected from the observable cracking behaviors to a great extent. Therefore, the authors are willing to first have a qualitative understanding on the tensile or shear properties of HCC on a macro scale. HCC did not show various crack initiation directions with respect to the pre-existing crack, which were controlled by the water pressure and

stress field around the crack tips. Moreover, these HCC generally inclined at an angle of about 10° – 15° and propagated nearly parallel with the confining compression direction and follow well-defined paths. These phenomena were very consistent with the cracking behaviors of tensile cracks. According to the Mohr-Coulomb yielding criterion, the angle between the shear failure plane and the minimum principal stress should be $45^{\circ} + \varphi/2$, where φ is the angle of internal friction angle of the specimen. In this study, φ is 30° , which indicates if HCC were shear cracks, the initiation direction should be 60° instead of 10° – 15° . Based on the above analysis on cracking initiation direction and propagation processes, HCCs are more like tensile cracks than shear cracks, and this further confirms that HCC are not a type of secondary cracks or anti-wing cracks.

To draw conclusion of the mechanical properties of HCC comprehensively, the fracture surfaces of them were investigated. Observing the HCC near the pre-existing crack, the fracture surface was clean and smooth, which indicated that a large number of tensile cracks appeared in this area. The HCC were tensile cracks at the initiation moment. However, when observing the HCC near the edges of the specimen, some rough and stepped fracture surfaces was found. In addition, many narrow zones consisting of small staggered cracks were observed around interface of HCC and specimen boundaries, which suggested that shear stress was concentrated at the end of the propagation processes. It can be inferred that a large number of shear cracks initiated and developed quickly at this time and the specimen failure was caused by the interaction of tensile cracks and shear cracks. Based on the above analysis on fracture surfaces, HCC are more like tensile and shear mixed cracks, which are different from tensile cracks.

The above macroscopic observations reveal that the HCC, which initiate and propagate under coupled hydro-mechanical effects, are different from tensile wing cracks, secondary cracks, and anti-wing cracks. They showed obvious tensile properties on initiation angles and cracking trajectories. However, many shear regions were observed on the fracture surfaces of HCC. The results were not satisfactory if only macroscopic investigations were conducted. Therefore, the following section will concentrate on the microscopic characteristics of HCC, and find out the mechanical properties of them.

4. Microscopic Study

As reported in the Section 3.1, the crack type of HCC cannot be confirmed on a macro scale. Therefore, this section deals with the microscopic aspects of the study. Specifically, the scanning electron microscope (SEM), Nova NanoSEM 450, which is housed in Tongji University since 2016, was adopted for this research.

4.1. Shear and Tensile Fracturing Zones

The first problem we need to solve is how to distinguish tensile and shear fractures on a micro scale. While many scholars have contributed on this problem [42–45], their outcomes cannot match our research due to the differences in specimen materials, observation equipment, and analysis methods. Therefore, the authors will illustrate the microscopic judgement methods (SFZ and TFZ) for tensile fracture and shear fracture in gypsum specimens.

As shown in Figure 5, where the magnification is 3000 times, the microscopic shear fractures and tensile fractures appear in the upper left and the lower right, respectively, and they perform quite differently. Firstly, in shear fracturing zone (SFZ), almost all the gypsum grains are in the same direction, which directly reflects the orientation of shear stress. Intuitively, the SFZ is smooth and neat. On the contrary, in tensile fracturing zone (TFZ), although many gypsum grains orient towards the outside plane, the directions are quite chaotic and irregular. The TFZ is observed to be rough and uneven. Moreover, the length of the gypsum grains are basically the same in SFZ, more than 80% of them are around $15\ \mu\text{m}$ long. However, in TFA, the length of the gypsum grains are different, ranging from $2\ \mu\text{m}$ to $12\ \mu\text{m}$. Third, there are no obvious boundary lines between many gypsum grains in SFZ, they are gathered together to form a larger grain set. This phenomenon

is caused by the simultaneous action of both compression stress and shear stress on the interfaces of grains, which reduces the gaps among grains. In contrast, the gypsum grains in TFZ are more independent, the boundary lines of them are obvious and there are a large number of gaps among grains. This phenomenon is caused by the tensile stress which applied in TFZ during the cracking processes, and many gaps are formed by tensile dislocation of grains. Based on the above judgement criteria, the tensile fracture and shear fracture can be separated easily and accurately on a micro scale using SEM system, and this is the basis of the further microscopic study. It is worth emphasizing that due to many other factors like stress statuses and boundary conditions, the micro characteristics of TFZ and SFZ are not equal to macroscopic characteristics of tensile cracks and shear cracks, which are presented in our previous studies [39,41].

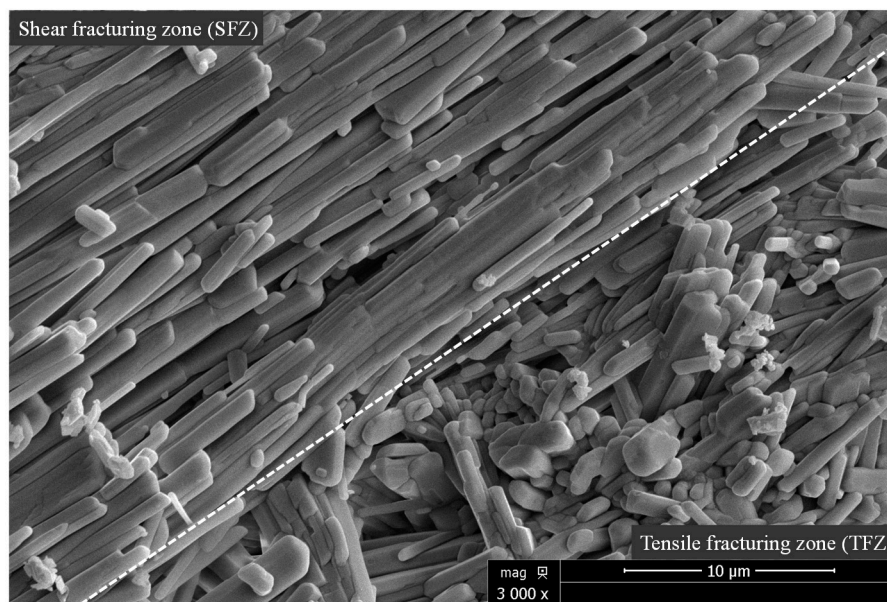


Figure 5. SEM scanning image of SFZ and TFZ.

4.2. Mechanical Properties of HCC

As reported before, the HCC only developed in the specimens with low inclination angles. In this section, the SEM tests were then carried out on the fracture surfaces of HCC in 15°, 30°, and 45° specimen. To help demonstrate the analysis method and reveal the mechanical properties of HCC, the authors select 30° specimen as a representative (Figure 6). As shown in Figure 6, two pieces of scanning specimens ($10 \times 5 \times 8 \text{ mm}^3$), S1 and S2, were trimmed down near the outer tip of the pre-existing crack and the edge of the specimen, respectively. Considering that when a new crack propagates to a certain region, this region will be damaged, and its structure will lose stability and can not bear any external loading. Therefore, the fracture surfaces will be well preserved, and final failure statuses of this region can directly reflect the mechanical properties of a segment of new crack. On this basis, it is regarded that S1 and S2 can reflect the tensile and shear properties of HCC when (1) it just initiated from the outer tip of pre-existing crack, and (2) it reached the edge of the specimen and led to the failure of the specimen.

Figure 7 is one of the SEM scanning areas of S1 with the magnification of 500 times. Nearly all the information of gypsum grains can be clearly observed, including their shapes, orientations, length, relative positions, and gaps among grains. Based on the judgment criteria in Section 4.1, the mechanical properties of this scanning area can be obtained from the following aspects. The orientations of grains are chaotic and irregular, more than half of them orient towards the outside plane. The overall observation feeling of this area is rough and uneven. Subsequently, the length of the grains are quite different, although more than 90% of them ranges from 2 μm to 12 μm , some grains are even longer than

50 μm , like Area A, which have been framed in the figure. Moreover, the grains in the scanning section are independent, the boundary lines and gaps among them are clearly enough. These characteristics indicate that this area is caused by tensile stress and exhibits obvious tensile fracture properties.

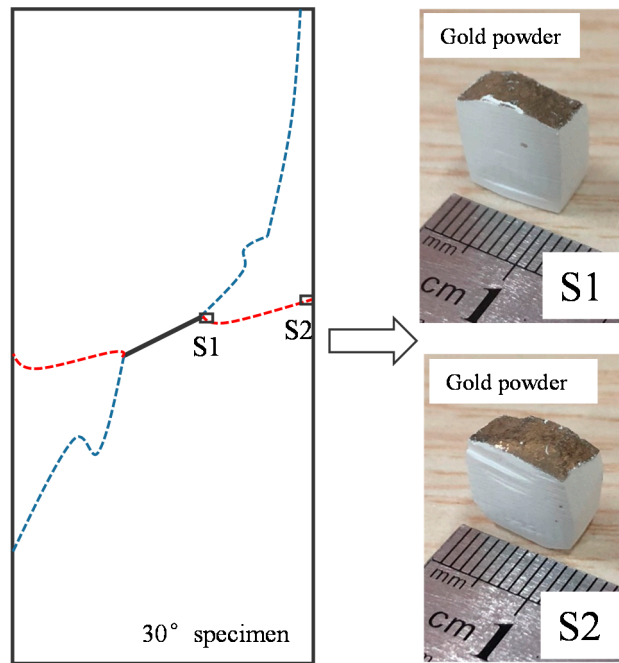


Figure 6. SEM scanning specimens of HCC in a 30° specimen.

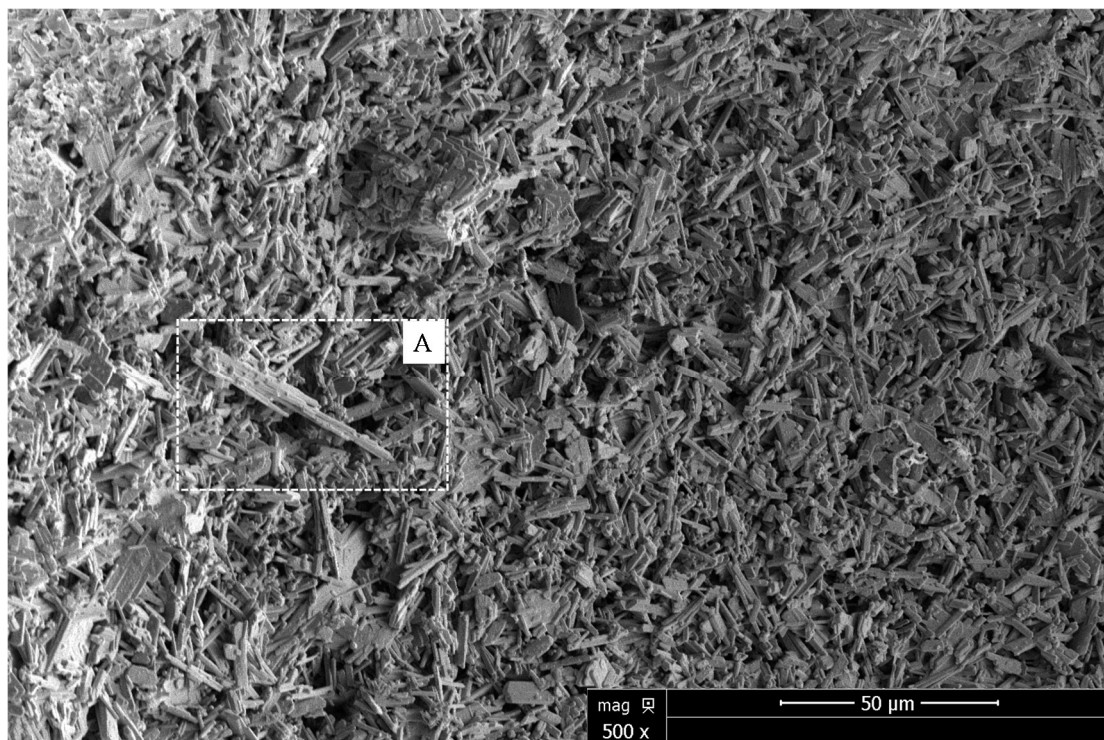


Figure 7. SEM scanning image of S1 (500 times).

For a further understanding of the stress states applied in this area, the authors magnified the observation multiple to 1000 times of Area A (Figure 8). In addition to the grain orientations, length, and gaps, a large number of debris are observed to be scattered randomly around the tips of gypsum

grains. These grain debris are caused by the pullout effect between the inlaid grains. While the applied pullout stress is not sufficient to reach the critical value of intergranular fracture, some debris will also occur with the relative displacement between the grains. The occurrence of scattered grain debris further confirms the tensile properties of this area.

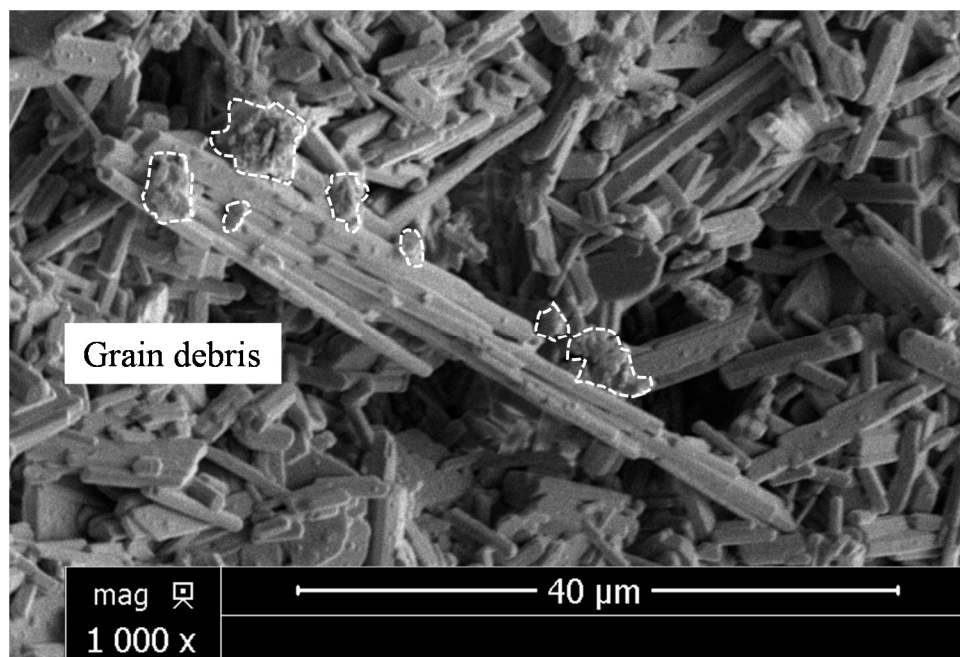


Figure 8. SEM scanning image of S1 (1000 times).

The authors then scanned the rest areas of S1 and found that the remaining areas are almost the same as Figure 7, all the scanning sections show obvious tensile properties, and no shear properties are observed. It can be concluded that only tensile stress, which was caused by the coupled hydro-mechanical effects, was applied on the S1. The water pressure has a significant influence on the internal stress state of coupled cracks compared with triaxial compression loading tests. At the initiation moment, the water pressure resisted the effect of confining pressure and enhanced the effect of vertical loading. The tensile stress around the pre-crack tip reached the critical tensile strength, and then led to the fracture of this area. As a summary, the coupled crack was a tensile crack when it just initiated from the outer tip of the pre-existing crack. This is consistent with the macroscopic observation.

Figure 9 is one of the SEM scanning areas of S2 with the magnification of 500 times. As presented before, all the detailed information, including grain shapes, orientations, and length can be observed. It can be investigated that more than 70% of the scanning areas are basically the same as Figure 7, which indicates that these areas were caused by tensile stress, and exhibit tensile fracture properties. However, nearly 30% of the scanning areas show different micro characteristics, like Area A and B. In order to study the mechanical properties of these areas more directly and precisely, the observation multiple of Area A was then magnified to 1000 times (Figure 10) and the center of the scanning section is highlighted. The following statements are all aimed at the center area. As shown in Figure 10, all the gypsum grains orient towards the same direction, the overall observation feeling of this area is smooth and neat. Subsequently, the length of grains are very uniform, more than 80% of them are around 15 μm . Moreover, there are no obvious boundary lines among many grains, most of them are gathered together to form a larger grain set, and the grain gaps are almost disappeared. Based on the judgment criteria in Section 4.1, this area was caused by shear stress and exhibits obvious shear fracture properties.

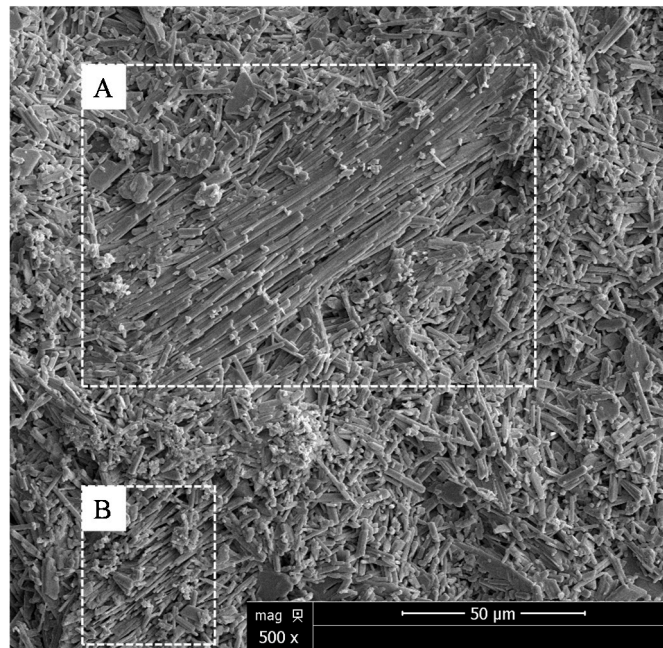


Figure 9. SEM scanning image of S2 (500 times).

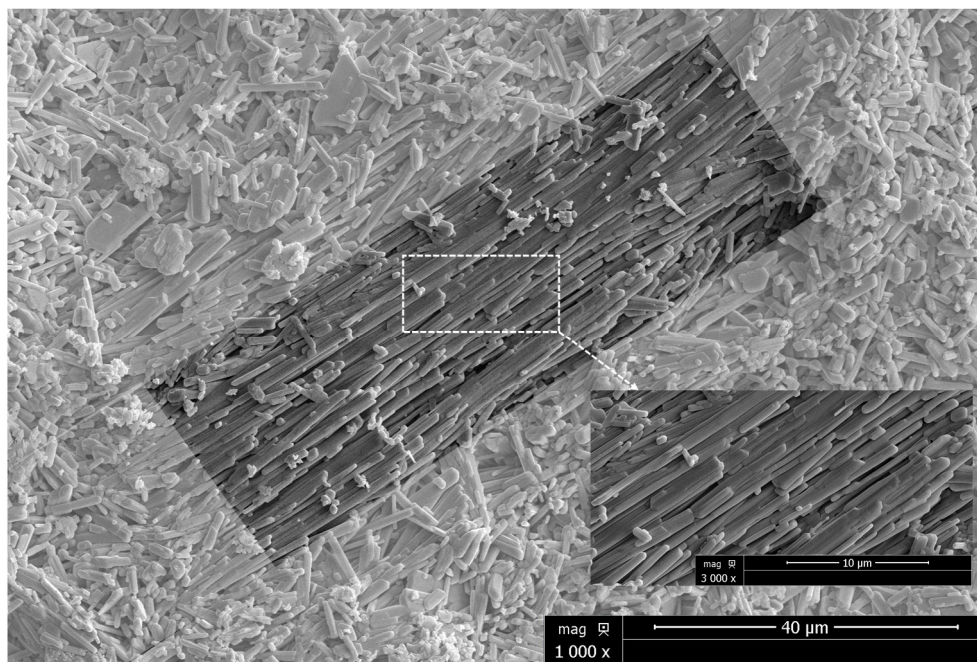


Figure 10. SEM scanning image of S2 (1000 times and 3000 times).

In order to further study the stress states applied in this SFZ and the distribution of grain debris, the authors continue to magnify Area A to 3000 times (Figure 10). Different from Figure 8, there is few grain debris appeared in the scanning area, and the surfaces of grains are flat and intact. This phenomenon indicates that there is only slippage displacement between gypsum grains without any pullout trend. The disappearance of grain debris further confirms the shear properties of this area.

The authors then scanned the rest areas of S2 and found that the remaining areas were almost the same as Figure 9. Although most of the scanning sections were caused by tensile stress, about 20–30% of the scanning sections showed shear fracture properties. It can be inferred that both tensile stress and shear stress were applied on the S2. At this critical moment of specimen failure, the coupled cracks propagated close to the edges of specimens. Compared with the initiation moment, the resistance

of water pressure to confining pressure is obviously reduced, which leads to the enhancement of the slippage deformation of crack surfaces. Moreover, due to the boundary effects, the confining pressure has a more important effect on the mechanical properties of coupled cracks. As a summary, the coupled crack was a mixed crack when it reached the edge of the specimen. This is consistent with the macroscopic observation.

With reference to Figures 7–10 and the above analysis, we can briefly describe the cracking processes of HCC under coupled hydro-mechanical effect. At the beginning of the loading test, the tensile stress highly concentrates around the outer tips of pre-existing crack. Subsequently, due to the water pressure, a horizontal coupled crack initiates when the tensile stress reaches the critical tensile strength of the specimen and gradually propagates towards the edges of the specimen. While tensile stress makes a major contribution to the crack propagation, shear stress gradually increases with the vertical loading. When the specimen is about to fail, the proportion of shear stress reaches 20–30%. Additionally, the coupled crack, which exhibit both tensile and shear fracturing properties simultaneously, is a mixed crack at this time. Meanwhile, the reason for the absence of HCC in 60° specimen and 75° specimen can also be explained. Many previous studies [40,46,47] have revealed that the external loading will favor further propagation of shear cracks in the specimens with steeply-inclined cracks. Considering that the HHC were tensile cracks when they initiated, the large inclination angles (60° and 75°) would strongly inhibit the occurrence of HCC.

5. Conclusions

In order to research the fracturing behaviors and mechanical properties of cracks under coupled hydraulic-mechanical effects, a series of triaxial compression loading tests on the cylinder gypsum specimens were carried out. The hydraulic pressure was injected into the specimens through a water channel. Microscopic investigations were then conducted on scanning pieces cut from the horizontal coupled cracks (HCC). Several conclusions are obtained from the macroscopic observation and microscopic analysis in the present study.

Comparing the test results of WP = 0 MPa and WP = 5 MPa, it is found that water pressure has a significant effect on the cracking trajectories of new cracks in the specimens with low inclination angles ($\alpha = 15^\circ, 30^\circ, \text{ and } 45^\circ$), but the influence on the specimens with high inclination angles ($\alpha = 60^\circ \text{ and } 75^\circ$) is not obvious. Specifically, several horizontal coupled cracks (HCC) will appear in 15°, 30°, and 45° specimens when water pressure is applied inside the pre-existing cracks. From the macroscopic observation on the initiation angles and fracture surfaces, HCC are different from tensile wing cracks, shear secondary cracks, and shear anti-wing cracks. Actually, they are unique cracks which are caused by the coupled hydraulic-mechanical effects.

On a micro scale, shear fracturing zones (SFZ) and tensile fracturing zones (TFZ) under coupled hydraulic-mechanical effects are separated from the aspects of orientations, length, and independence of gypsum grains. Based on the microscopic observation, HHC are not the cracks with a single mechanical property. When they just initiate from the outer tips of pre-existing cracks, they are tensile cracks. However, when they reach the edges of the specimens, they become tensile and shear mixed cracks. While tensile stress, which is applied by the hydraulic pressure and external loading, makes a significant contribution to the specimen failure during the whole cracking processes, the effect of shear stress in HCC cannot be ignored.

Author Contributions: Conceptualization, C.Z. (Cheng Zhao); methodology, C.Z. (Cheng Zhao); validation, C.Z. (Cheng Zhao) and C.Z. (Chunfeng Zhao); formal analysis, Y.Z.; investigation, Y.Z. and C.M.; data curation, Y.Z. and J.X.; writing—original draft preparation, Y.Z.; writing—review and editing, C.Z. (Cheng Zhao) and C.Z. (Chunfeng Zhao); supervision, C.Z. (Cheng Zhao) and C.Z. (Chunfeng Zhao); project administration, C.Z. (Cheng Zhao); funding acquisition, C.Z. (Cheng Zhao).

Funding: This research was funded by [the National Key Research and Development Plan] grant number (2017YFC0806000), [the National Natural Science Foundation of China] grant number (41202193, 41572262), and (Shanghai Rising-Star Program) grant number (17QC1400600).

Conflicts of Interest: The authors declare no conflict of interest. The funders had no role in the design of the study; in the collection, analyses, or interpretation of data; in the writing of the manuscript, and in the decision to publish the results.

References

1. Gonçalves da Silva, B.; Einstein, H.H. Physical processes involved in the laboratory hydraulic fracturing of granite: Visual observation and interpretation. *Eng. Fract. Mech.* **2018**, *191*, 125–142. [[CrossRef](#)]
2. Warpinsky, N.R.; Clark, J.A.; Schmidt, R.A.; Huddle, C.W. Laboratory investigation on the effect of in-situ stresses on hydraulic fracture containment. *Soc. Pet. Eng. J.* **1982**, *22*, 333–340. [[CrossRef](#)]
3. Song, I.; Suh, M.; Won, K.S. A laboratory study of hydraulic fracturing breakdown pressure in table rock sandstone. *Geosci. J.* **2001**, *5*, 263–271. [[CrossRef](#)]
4. Stanchits, S.; Mayr, S.; Shapiro, S.; Dresen, G. Fracturing of porous rock induced by fluid injection. *Tectonophysics* **2011**, *503*, 129–145. [[CrossRef](#)]
5. Li, B.; Wong, R.C.K.; Milnes, T. Anisotropy in capillary invasion and fluid flow through induced sandstone and shale fractures. *Int. J. Rock Mech. Min.* **2014**, *65*, 129–140. [[CrossRef](#)]
6. Guo, C.; Xu, J.; Wei, M.; Jiang, R. Experimental study and numerical simulation of hydraulic fracturing tight sandstone reservoirs. *Fuel* **2015**, *159*, 334–344. [[CrossRef](#)]
7. Zhao, J.; Pu, X.; Li, Y.; He, X. A semi-analytical mathematical model for predicting well performance of a multistage hydraulically fractured horizontal well in naturally fractured tight sandstone gas reservoir. *J. Nat. Gas Sci. Eng.* **2016**, *32*, 273–291. [[CrossRef](#)]
8. He, J.M.; Lin, C.; Li, X.; Zhang, Y.; Chen, Y. Initiation, propagation, closure and morphology of hydraulic fractures in sandstone cores. *Fuel* **2017**, *208*, 65–70. [[CrossRef](#)]
9. Rodriguez, I.V.; Stanchits, S. Spatial and temporal variation of seismic attenuation during hydraulic fracturing of a sandstone block subjected to triaxial stress. *J. Geophys. Res. Solid Earth* **2017**, *122*, 9012–9030. [[CrossRef](#)]
10. Warpinski, N.R.; Teufel, L.W. Influence of geologic discontinuities on hydraulic fracture propagation. *J. Pet. Technol.* **1987**, *39*, 209–220. [[CrossRef](#)]
11. Blair, S.C.; Thorpe, R.K.; Heuze, F.E.; Shaffer, R.J. Laboratory observations of the effect of geological discontinuities on hydrofracture propagation. In Proceedings of the 30th US Symposium on Rock Mechanics, Morgantown, WV, USA, 19–22 June 1989; pp. 433–450.
12. Damani, A.; Sharma, A.; Sondergeld, C.H.; Rai, C.S. Acoustic mapping and microscopic analysis of laboratory induced hydraulic fractures under triaxial stress conditions. In Proceedings of the 47th US Rock Mechanics/Geomechanics Symposium, San Francisco, CA, USA, 23–26 June 2013.
13. Wanniarachchi, W.A.M.; Gamage, R.P.; Perera, M.S.A.; Rathnaweera, T.D.; Gao, M.; Padmanabhan, E. Investigation of depth and injection pressure effects on breakdown pressure and fracture permeability of shale reservoirs: An experimental study. *Appl. Sci.* **2017**, *7*, 664. [[CrossRef](#)]
14. Renard, F.; Bernard, D.; Desrues, J.; Ougier-Simonin, A. 3D imaging of fracture propagation using synchrotron X-ray microtomography. *Earth Planet. Sci. Lett.* **2009**, *286*, 285–291. [[CrossRef](#)]
15. Pradhan, S.; Stroisz, A.M.; Fjær, E.; Stenebråten, J.F.; Lund, H.K.; Sønstebo, E.F. Stress-induced fracturing of reservoir rocks: Acoustic monitoring and CT image analysis. *Rock Mech. Rock Eng.* **2015**, *48*, 2529–2540. [[CrossRef](#)]
16. Liu, S.; Harpalani, S. Permeability prediction of coalbed methane reservoirs during primary depletion. *Int. J. Coal Geol.* **2012**, *113*, 1–10. [[CrossRef](#)]
17. Orem, W.; Tatu, C.; Varonka, M.; Lerch, H.; Bates, A.; Engle, M.; Crosby, L.; McIntosh, J. Organic substances in produced and formation water from unconventional natural gas extraction in coal and shale. *Int. J. Coal Geol.* **2014**, *126*, 20–31. [[CrossRef](#)]
18. Blanton, T.L. Propagation of hydraulically and dynamically induced fractures in naturally fractured reservoirs. In Proceedings of the SPE/DOE Unconventional Gas Technology Symposium, Louisville, KY, USA, 18–21 May 1986.
19. Fisher, M.K.; Wright, C.A.; Davidson, B.M.; Steinsberger, N.P.; Buckler, W.S.; Goodwin, A.; Fielder, E.O. Integrating fracture mapping technologies to improve stimulations in the Barnett shale. *SPE Prod. Facil.* **2005**, *20*, 85–93. [[CrossRef](#)]

20. Li, X.; Feng, Z.; Han, G.; Elsworth, D.; Marone, C.; Saffer, D.; Cheon, D.S. Breakdown pressure and fracture surface morphology of hydraulic fracturing in shale with H₂O, CO₂ and N₂. *Geomech. Geophys. Geo-Energy Geo-Resour.* **2016**, *2*, 63–76. [[CrossRef](#)]
21. Lin, C.; He, J.M.; Li, X.; Wan, X.; Zheng, B. An experimental investigation into the effects of the anisotropy of shale on hydraulic fracture propagation. *Rock Mech. Rock Eng.* **2017**, *50*, 543–554. [[CrossRef](#)]
22. Lin, C.; He, J.M.; Li, X. Width Evolution of the hydraulic fractures in different reservoir rocks. *Rock Mech. Rock Eng.* **2018**, *51*, 1621–1627. [[CrossRef](#)]
23. Chen, Z.; Narayan, S.P.; Yang, Z.; Rahman, S.S. An experimental investigation of hydraulic behaviour of fractures and joints in granitic rock. *Int. J. Rock Mech. Min. Sci.* **2000**, *37*, 1061–1071. [[CrossRef](#)]
24. Shao, H.; Kabilan, S.; Stephens, S.; Suresh, N.; Beck, A.N.; Varga, T.; Martin, P.F.; Kuprat, A.; Jung, H.B.; Um, W.; et al. Environmentally friendly, rheoreversible, hydraulic-fracturing fluids for enhanced geothermal systems. *Geothermics* **2015**, *58*, 22–31. [[CrossRef](#)]
25. Chen, Y.; Nagaya, Y.; Ishida, T. Observations of fractures induced by hydraulic fracturing in anisotropic granite. *Rock Mech. Rock Eng.* **2015**, *48*, 1455–1461. [[CrossRef](#)]
26. Gonçalves da Silva, B.; Einstein, H.H.; Li, B.Q.; Moradian, Z.; Germaine, J.T.; Einstein, H.H. Development of a test setup capable of producing hydraulic fracturing in the laboratory with image and acoustic emission monitoring. In Proceedings of the 49th US Rock Mechanics/Geomechanics Symposium, San Francisco, CA, USA, 28 June–1 July 2015.
27. Mao, R.B.; Feng, Z.J.; Liu, Z.H.; Zhao, Y. Laboratory hydraulic fracturing test on large-scale pre-cracked granite specimens. *J. Nat. Gas Sci. Eng.* **2017**, *44*, 278–286. [[CrossRef](#)]
28. Zhou, C.B.; Wan, Z.J.; Zhang, Y.; Gu, B. Experimental study on hydraulic fracturing of granite under thermal shock. *Geothermics* **2018**, *71*, 146–155. [[CrossRef](#)]
29. Blanton, T.L. An experimental study of interaction between hydraulically induced and pre-existing fractures. In Proceedings of the SPE/DOE Unconventional Gas Recovery Symposium, Pittsburgh, PA, USA, 16–18 May 1982.
30. Papadopoulos, J.M.; Narendran, V.M.; Cleary, M.P. Laboratory Simulations of Hydraulic Fracturing. In Proceedings of the SPE-11618-MS SPE/DOE Low Permeability Gas Reservoirs Symposium, Denver, CO, USA, 14–16 March 1983.
31. Depater, C.J.; Cleary, M.P.; Quinn, T.S. Experimental verification of dimensional analysis for hydraulic fracturing. *SPE Prod. Facil.* **1994**, *9*, 230–238. [[CrossRef](#)]
32. Fallahzadeh, S.H.; Rasouli, V.; Sarmadivaleh, M. An investigation of hydraulic fracturing initiation and near-wellbore propagation from perforated boreholes in tight formations. *Rock Mech. Rock Eng.* **2015**, *48*, 573–584. [[CrossRef](#)]
33. Liu, R.C.; Jiang, Y.J.; Li, B.; Yu, L. Estimating permeability of porous media based on modified Hagen–Poiseuille flow in tortuous capillaries with variable lengths. *Microfluid* **2016**, *20*, 120. [[CrossRef](#)]
34. Li, B.; Liu, R.C.; Jiang, Y.J. Influences of hydraulic gradient, surface roughness, intersecting angle, and scale effect on nonlinear flow behavior at single fracture intersections. *J. Hydrol.* **2016**, *538*, 440–453. [[CrossRef](#)]
35. Zhou, J.; Chen, M.; Jin, Y.; Zhang, G.Q. Analysis of fracture propagation behavior and fracture geometry using a tri-axial fracturing system in naturally fractured reservoirs. *Int. J. Rock Mech. Min. Sci.* **2008**, *45*, 1143–1152. [[CrossRef](#)]
36. Zhou, J.; Jin, Y.; Chen, M. Experimental investigation of hydraulic fracturing in random naturally fractured blocks. *Int. J. Rock Mech. Min. Sci.* **2010**, *47*, 1193–1199. [[CrossRef](#)]
37. Amalokwu, K.; Best, A.; Sothcott, J.; Chapman, M.; Minshull, T.; Li, X.Y. Water saturation effects on elastic wave attenuation in porous rocks with aligned fractures. *Geophys. J. Int.* **2014**, *197*, 943–947. [[CrossRef](#)]
38. Liu, R.C.; Jing, H.W.; He, L.X. An experimental study of the effect of fillings on hydraulic properties of single fractures. *Environ. Earth Sci.* **2017**, *76*, 684. [[CrossRef](#)]
39. Zhao, C.; Ma, C.C.; Zhao, C.F.; Du, S.; Bao, C. Crack propagation simulation of rock-like specimen using strain criterion. *Eur. J. Environ. Civ. Eng.* **2017**, 1–18. [[CrossRef](#)]
40. Wong, L.N.Y.; Einstein, H.H. Systematic evaluation of cracking behavior in specimens containing single flaws under uniaxial compression. *Int. J. Rock Mech. Min. Sci.* **2009**, *46*, 239–249. [[CrossRef](#)]
41. Zhao, C.; Zhou, Y.M.; Zhao, C.F.; Bao, C. Cracking process and coalescence modes in rock-like specimens with two parallel pre-existing cracks. *Rock Mech. Rock Eng.* **2018**, 1–17. [[CrossRef](#)]

42. Huang, J.F.; Chen, G.G.; Zhao, Y.H.; Wang, R. An experimental study of the strain field development prior to failure of a marble plate under compression. *Tectonophysics* **1990**, *175*, 269–284.
43. Sagong, M.; Bobet, A. Micro-fractographic characterization of tensile and shear cracks. In Proceedings of the Soil and Rock America Symposium, Cambridge, MA, USA, 22–26 June 2003; pp. 937–944.
44. Wong, L.N.Y.; Einstein, H.H. Crack coalescence in molded gypsum and Carrara marble: Part 2. Microscopic observations and interpretation. *Rock Mech. Rock Eng.* **2009**, *42*, 513–545. [[CrossRef](#)]
45. Cheng, Y.; Wong, L.N.Y. Microscopic characterization of tensile and shear fracturing in progressive failure in marble. *J. Geophys. Res. Solid Earth* **2018**, *123*, 204–225. [[CrossRef](#)]
46. Li, H.Q.; Wong, L.N.Y. Influence of flaw inclination angle and loading condition on crack initiation and propagation. *Int. J. Solids Struct.* **2012**, *49*, 2482–2499. [[CrossRef](#)]
47. Yang, L.; Jiang, Y.J.; Li, B.; Li, S.; Gao, Y. Application of the expanded distinct element method for the study of crack growth in rock-like materials under uniaxial compression. *Front. Struct. Civ. Eng.* **2012**, *6*, 121–131. [[CrossRef](#)]



© 2018 by the authors. Licensee MDPI, Basel, Switzerland. This article is an open access article distributed under the terms and conditions of the Creative Commons Attribution (CC BY) license (<http://creativecommons.org/licenses/by/4.0/>).